Extended Measurements of Cosmic-ray Electron and Positron Spectrum from 11 GeV to 4.8 TeV with the Calorimetric Electron Telescope on the International Space Station Supplemental online material.

(CALET Collaboration)

(Dated: May 21, 2018)

Supplemental material concerning "Extended Measurements of Cosmic-ray Electron and Positron Spectrum from 11 GeV to 4.8 TeV with the Calorimetric Electron Telescope on the International Space Station."

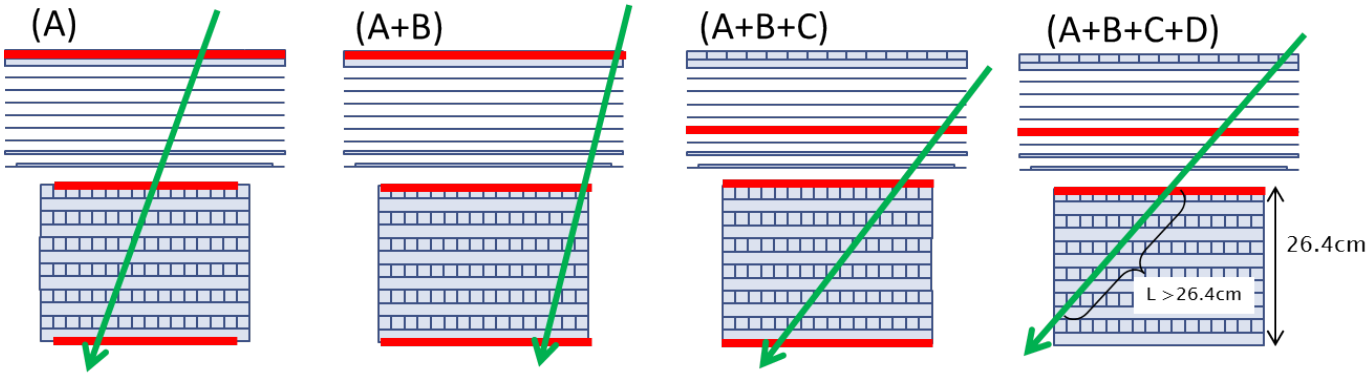

FIG. 1. Classification of four geometrical condition types. The red bars indicate the geometrical requirements for the particle trajectory at different detector layers. In each of the plots, the green arrow shows an example of a shower axis which is allowed by the extention of the geometrical condition. Geometrical condition A requires the shower axis to cross the TASC top and bottom layers except for a 2 cm outer margin, while in geometrical condition A+B the shower axis is allowed to cross the edge of TASC. In geometrical condition A+B+C, incidence from the side is allowed, but passage through the IMC 5th layer is required. Geometrical condition A+B+C+D does not require crossing of the TASC bottom layer, but it is required that the track length in TASC is greater than 26.4 cm. Each of A, B, C and D are defined exclusively, e.g. an event fulfilling condition A is not listed as fulfilling condition B as well.

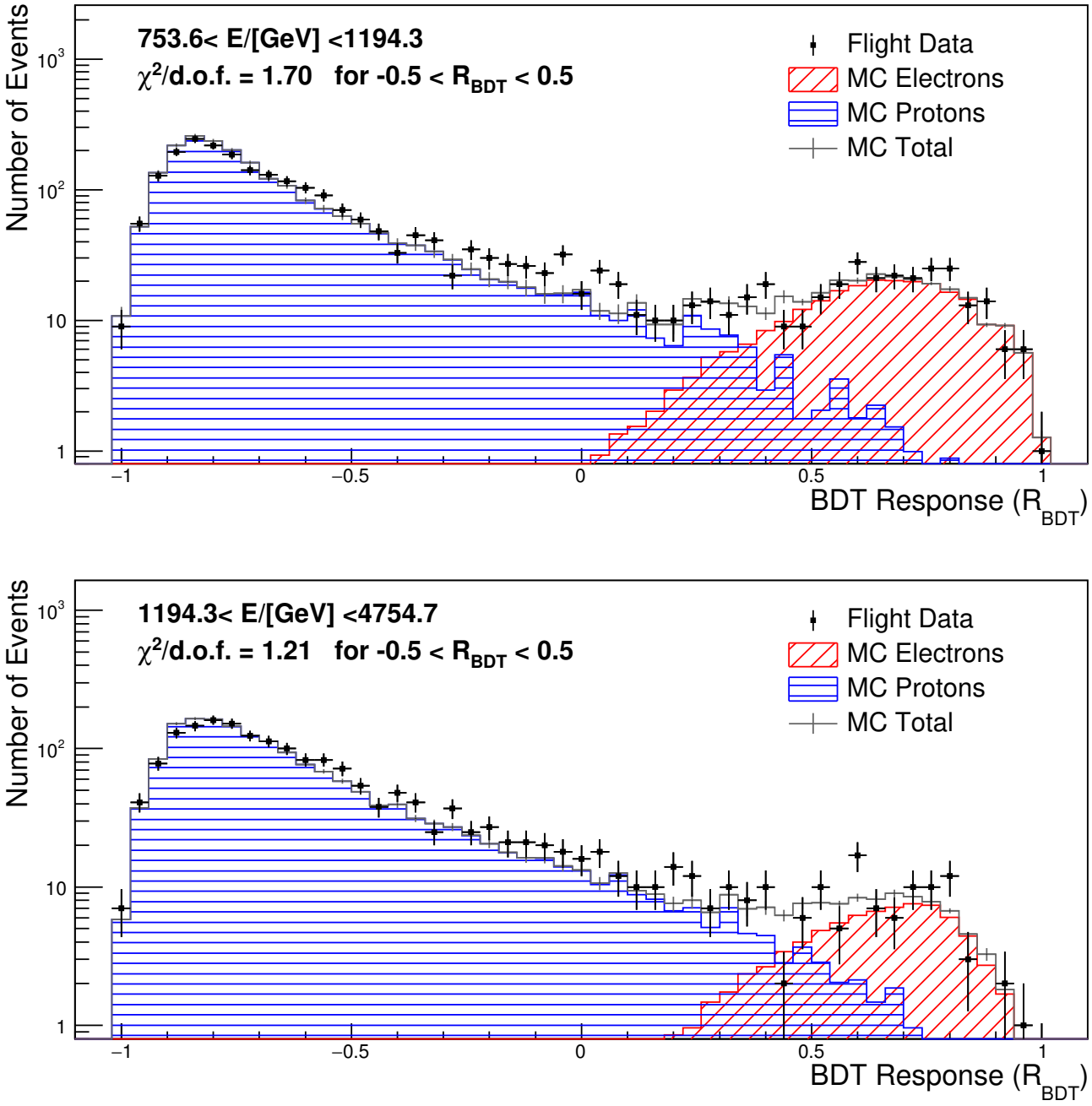

FIG. 2. Examples of BDT response ($R_{\rm BDT}$) distributions in the $754 < E < 1194$ GeV (*Top*) and $1194 < E < 4575$ GeV (*Bottom*) bins including all acceptance conditions A, B, C and D. While there is noticeable discrepancies in the $-0.3 < R_{\rm BDT} < 0$ region, their possible effects to the resultant spectrum are included in the systematic uncertainty concerning the BDT stability.

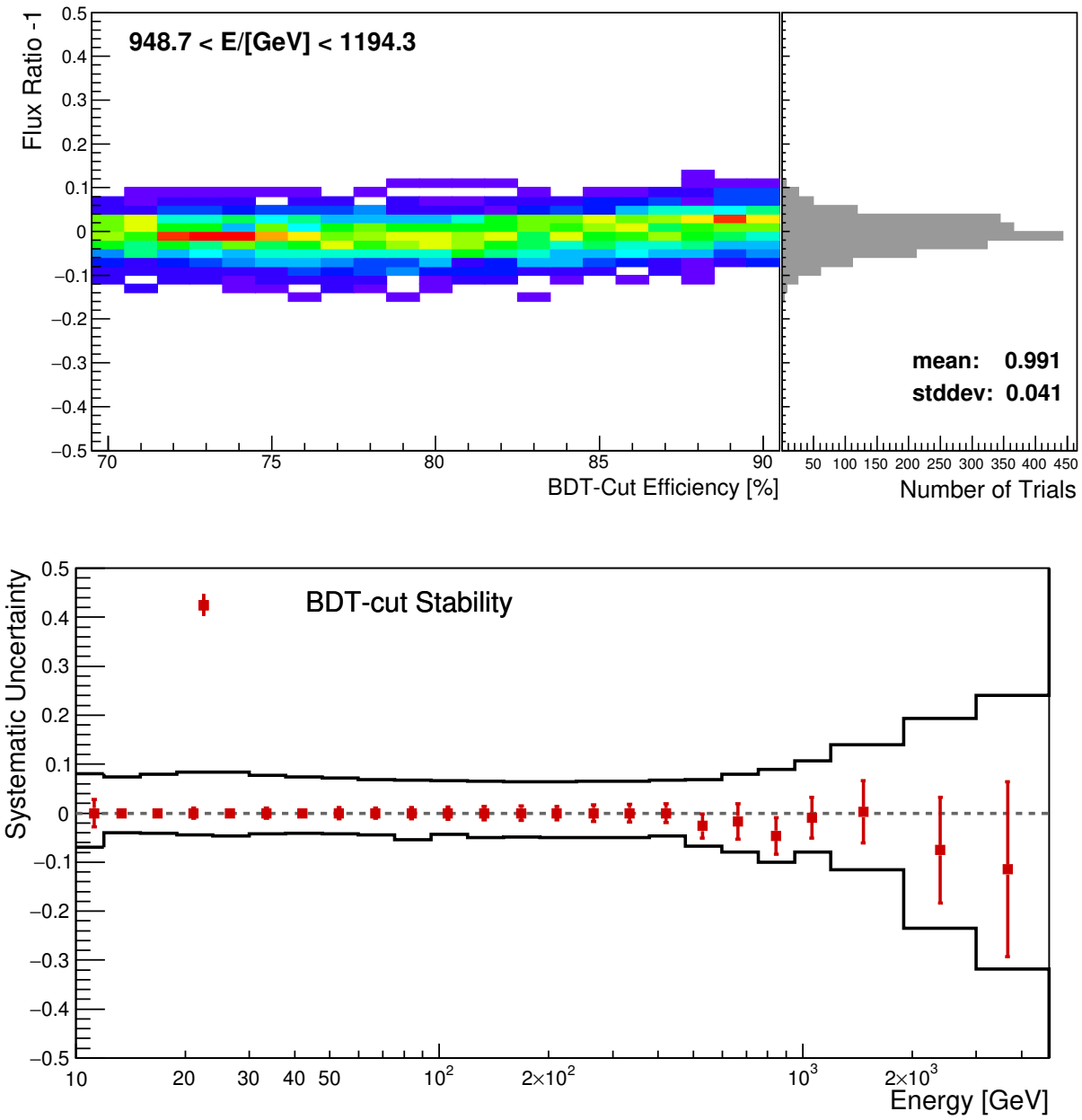

FIG. 3. (*Top*) Stability of BDT analysis with respect to independent training samples and BDT-cut efficiency in the $949 < E < 1194$ GeV bin. Color maps show the flux ratio dependence on efficiency, where the bin value (number of trials) increases as color changes from violet, blue, green, yellow to red. A projection onto the Y-axis is shown as a rotated histogram (in gray color). (*Bottom*) Energy dependence of systematic uncertainties. The red squares represent the systematic uncertainties stemming from the electron identification based on BDT. The bands defined by black lines show the sum in quadrature of all the sources of systematics, except the energy scale uncertainties.

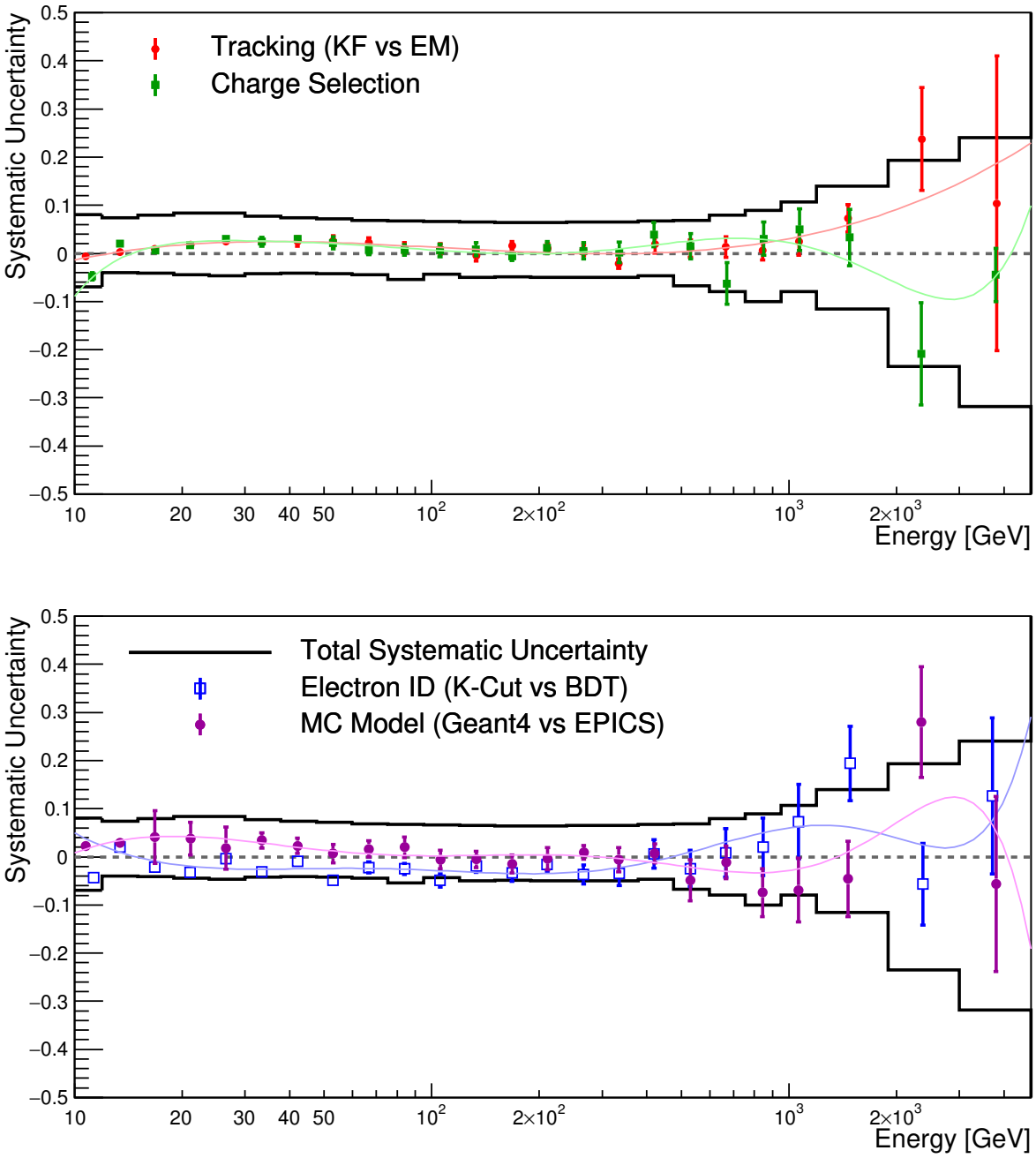

FIG. 4. (*Top*) Energy dependence of systematic uncertainties in tracking algorithms (Electromagnetic shower tracking vs combinatorial Kalman filter tracking) and charge identification methods (CHD vs IMC), (*Bottom*) Energy dependence of systematic uncertainties in electron identification methods (K-estimator vs BDT) and MC models (Geant4 vs EPICS). The data points are fitted with log-polynomial functions to mitigate the effect of statistical fluctuations while preserving possible energy dependent structures. Fit functions are shown as curves and are used to estimate energy dependent systematic uncertainties.

TABLE I. Table of CALET electron plus positron spectrum. Mean energy is calculated using the candidate events in the energy bin. For the flux the first and second errors represent the statistical uncertainties (68% confidence level) and systematic uncertainties, respectively, while uncertainty in the energy scale is not included. Detailed breakdown of systematic errors is included where $\sigma_{\rm BDT}$, $\sigma_{\rm trig.}$, $\Delta_{\rm norm.}$, $\Delta_{\rm trk.}$, $\Delta_{\rm chg.}$, $\Delta_{\rm ID}$ and $\Delta_{\rm MC}$ denote systematic errors due to BDT stability, trigger, absolute normalization, tracking, charge identification, electron identification, and MC model dependence, respectively. While the first two components must be added in quadrature to the statistical errors in the spectral analysis, the latter five contributions could be treated as nuisance parameters, by introducing correction factors corresponding to each component. Energy dependence (or non-dependence) of each contribution is already determined, constraining the possible corrections due to the nuisance parameters. Although $\Delta_{\rm norm.}$ can be ignored in a spectral study only using CALET data, it should also be treated as a nuisance parameter in a combined analysis with the positron spectrum, for example.

Energy Bin	Mean Energy	Flux	Systematic Uncertainties (relative to flux)						
(GeV)	(GeV)	$(\mathrm{m^{-2}sr^{-1}s^{-1}GeV^{-1}})$	$\sigma_{\rm BDT}$	$\sigma_{\rm trig.}$	$\Delta_{\rm norm.}$	$\Delta_{\rm trk.}$	$\Delta_{\rm chg.}$	$\Delta_{\rm ID}$	$\Delta_{\rm MC}$
10.6–11.9	11.3	$(1.543 \pm 0.004^{+0.094}_{-0.106}) \times 10^{-1}$	0.028	0.024	0.032	-0.006	-0.048	0.031	0.021
11.9–13.4	12.6	$(1.065 \pm 0.003^{+0.057}_{-0.049}) \times 10^{-1}$	0.010	0.024	0.032	0.000	-0.021	0.016	0.030
13.4–15.0	14.2	$(7.388 \pm 0.023^{+0.410}_{-0.305}) \times 10^{-2}$	0.010	0.024	0.032	0.006	-0.003	0.004	0.037
15.0–16.9	15.9	$(5.073 \pm 0.018^{+0.302}_{-0.211}) \times 10^{-2}$	0.010	0.024	0.032	0.011	0.010	-0.005	0.041
16.9–18.9	17.8	$(3.521 \pm 0.014^{+0.223}_{-0.152}) \times 10^{-2}$	0.010	0.024	0.032	0.014	0.018	-0.013	0.043
18.9–21.2	20.0	$(2.468 \pm 0.011^{+0.162}_{-0.111}) \times 10^{-2}$	0.010	0.024	0.032	0.018	0.022	-0.018	0.043
21.2–23.8	22.5	$(1.687 \pm 0.008^{+0.112}_{-0.079}) \times 10^{-2}$	0.010	0.024	0.032	0.020	0.025	-0.022	0.041
23.8–26.7	25.2	$(1.171 \pm 0.006^{+0.077}_{-0.055}) \times 10^{-2}$	0.008	0.024	0.032	0.022	0.026	-0.024	0.038
26.7–30.0	28.3	$(8.029 \pm 0.034^{+0.516}_{-0.385}) \times 10^{-3}$	0.008	0.024	0.032	0.023	0.026	-0.025	0.035
30.0–33.7	31.7	$(5.413 \pm 0.026^{+0.313}_{-0.229}) \times 10^{-3}$	0.011	0.000	0.032	0.024	0.026	-0.026	0.031
33.7–37.8	35.6	$(3.721 \pm 0.020^{+0.206}_{-0.157}) \times 10^{-3}$	0.011	0.000	0.032	0.025	0.025	-0.026	0.026
37.8–42.4	39.9	$(2.612 \pm 0.016^{+0.137}_{-0.109}) \times 10^{-3}$	0.010	0.000	0.032	0.024	0.024	-0.025	0.022
42.4–47.5	44.8	$(1.798 \pm 0.013^{+0.090}_{-0.075}) \times 10^{-3}$	0.010	0.000	0.032	0.024	0.023	-0.025	0.018
47.5–53.3	50.3	$(1.255 \pm 0.010^{+0.060}_{-0.052}) \times 10^{-3}$	0.011	0.000	0.032	0.023	0.021	-0.024	0.014
53.3–59.9	56.4	$(8.863 \pm 0.078^{+0.404}_{-0.367}) \times 10^{-4}$	0.011	0.000	0.032	0.022	0.019	-0.024	0.010
59.9–67.2	63.3	$(6.157 \pm 0.061^{+0.266}_{-0.254}) \times 10^{-4}$	0.010	0.000	0.032	0.020	0.017	-0.024	0.007
67.2–75.4	71.0	$(4.188 \pm 0.048^{+0.173}_{-0.174}) \times 10^{-4}$	0.010	0.000	0.032	0.019	0.015	-0.025	0.005
75.4–84.6	79.7	$(2.984 \pm 0.038^{+0.119}_{-0.126}) \times 10^{-4}$	0.012	0.000	0.032	0.017	0.012	-0.025	0.003
84.6–94.9	89.4	$(2.032 \pm 0.030^{+0.078}_{-0.087}) \times 10^{-4}$	0.012	0.000	0.032	0.015	0.010	-0.027	0.002
94.9–106.4	100.4	$(1.45 \pm 0.02^{+0.05}_{-0.06}) \times 10^{-4}$	0.013	0.000	0.032	0.013	0.007	-0.028	0.002
106.4–119.4	112.6	$(9.82 \pm 0.18^{+0.36}_{-0.45}) \times 10^{-5}$	0.013	0.000	0.032	0.011	0.005	-0.030	0.002
119.4–134.0	126.2	$(6.98 \pm 0.15^{+0.25}_{-0.33}) \times 10^{-5}$	0.014	0.000	0.032	0.009	0.003	-0.031	0.003
134.0–150.4	141.7	$(4.93 \pm 0.12^{+0.18}_{-0.24}) \times 10^{-5}$	0.014	0.000	0.032	0.007	0.001	-0.033	0.003
150.4–168.7	159.0	$(3.47 \pm 0.09^{+0.12}_{-0.17}) \times 10^{-5}$	0.014	0.000	0.032	0.005	-0.000	-0.034	0.004
168.7–189.3	178.8	$(2.48 \pm 0.07^{+0.09}_{-0.12}) \times 10^{-5}$	0.014	0.000	0.032	0.003	-0.001	-0.035	0.004
189.3–212.4	200.1	$(1.69 \pm 0.06^{+0.06}_{-0.08}) \times 10^{-5}$	0.014	0.000	0.032	0.002	-0.001	-0.035	0.004
212.4–238.3	224.4	$(1.20 \pm 0.04^{+0.04}_{-0.06}) \times 10^{-5}$	0.014	0.000	0.032	0.001	0.000	-0.034	0.004
238.3–267.4	252.5	$(8.06 \pm 0.35^{+0.29}_{-0.39}) \times 10^{-6}$	0.017	0.000	0.032	-0.000	0.002	-0.032	0.003
267.4–300.0	282.9	$(5.88 \pm 0.28^{+0.21}_{-0.27}) \times 10^{-6}$	0.017	0.000	0.032	-0.001	0.005	-0.029	0.001
300.0–336.6	317.4	$(4.05 \pm 0.22^{+0.15}_{-0.18}) \times 10^{-6}$	0.018	0.000	0.032	-0.001	0.008	-0.025	-0.002
336.6–377.7	355.6	$(2.73 \pm 0.17^{+0.10}_{-0.11}) \times 10^{-6}$	0.018	0.000	0.032	-0.000	0.012	-0.019	-0.005
377.7–423.8	400.4	$(1.74 \pm 0.13^{+0.07}_{-0.07}) \times 10^{-6}$	0.019	0.000	0.032	0.000	0.016	-0.012	-0.010
423.8–475.5	447.7	$(1.19 \pm 0.10^{+0.05}_{-0.05}) \times 10^{-6}$	0.019	0.000	0.032	0.002	0.020	-0.004	-0.014
475.5–598.6	529.3	$(6.90 \pm 0.40^{+0.29}_{-0.44}) \times 10^{-7}$	$^{+0.000}_{-0.051}$	0.000	0.032	0.005	0.026	0.010	-0.021
598.6–753.6	666.3	$(3.27 \pm 0.25^{+0.19}_{-0.22}) \times 10^{-7}$	$^{+0.019}_{-0.053}$	0.000	0.032	0.011	0.031	0.030	-0.030
753.6–948.7	843.7	$(1.74 \pm 0.16^{+0.12}_{-0.17}) \times 10^{-7}$	$^{+0.000}_{-0.083}$	0.000	0.032	0.021	0.029	0.050	-0.033
948.7–1194.3	1063.6	$(8.84 \pm 1.02^{+0.77}_{-0.57}) \times 10^{-8}$	$^{+0.032}_{-0.051}$	0.000	0.032	0.035	0.018	0.063	-0.025
1194.3–1892.9	1463.2	$(2.04 \pm 0.30^{+0.23}_{-0.14}) \times 10^{-8}$	$^{+0.066}_{-0.061}$	0.000	0.032	0.059	-0.015	0.062	0.010
1892.9–3000.0	2336.2	$(4.19 \pm 1.14^{+0.67}_{-0.85}) \times 10^{-9}$	$^{+0.032}_{-0.183}$	0.000	0.032	0.110	-0.083	0.026	0.102
3000.0–4754.7	3815.3	$(9.36^{+5.37}_{-4.47}{}^{+2.11}_{-2.79}) \times 10^{-10}$	$^{+0.064}_{-0.293}$	0.000	0.032	0.187	-0.045	0.090	0.051

TABLE II. Table of CALET electron plus positron spectrum using the same energy binning as the DAMPE spectrum. The tabulated information is the same as the previous table.

Energy Bin	Mean Energy	Flux	Systematic Uncertainties (relative to flux)						
(GeV)	(GeV)	$(m^{-2}sr^{-1}s^{-1}GeV^{-1})$	σ_{BDT}	$\sigma_{trig.}$	$\Delta_{norm.}$	$\Delta_{trk.}$	$\Delta_{chg.}$	Δ_{ID}	Δ_{MC}
10.6–12.2	11.4	$(1.526 \pm 0.004^{+0.093}_{-0.103}) \times 10^{-1}$	0.028	0.024	0.032	-0.006	-0.046	0.030	0.022
12.2–13.9	13.0	$(9.930 \pm 0.027^{+0.533}_{-0.439}) \times 10^{-2}$	0.010	0.024	0.032	0.002	-0.016	0.013	0.032
13.9–16.0	14.9	$(6.277 \pm 0.019^{+0.358}_{-0.258}) \times 10^{-2}$	0.010	0.024	0.032	0.008	0.003	-0.000	0.039
16.0–18.3	17.0	$(4.028 \pm 0.014^{+0.250}_{-0.171}) \times 10^{-2}$	0.010	0.024	0.032	0.013	0.015	-0.010	0.042
18.3–20.9	19.5	$(2.650 \pm 0.010^{+0.173}_{-0.118}) \times 10^{-2}$	0.010	0.024	0.032	0.017	0.022	-0.017	0.043
20.9–24.0	22.4	$(1.701 \pm 0.008^{+0.113}_{-0.079}) \times 10^{-2}$	0.010	0.024	0.032	0.020	0.025	-0.022	0.041
24.0–27.5	25.6	$(1.114 \pm 0.006^{+0.073}_{-0.053}) \times 10^{-2}$	0.008	0.024	0.032	0.022	0.026	-0.024	0.038
27.5–31.6	29.4	$(7.059 \pm 0.028^{+0.449}_{-0.339}) \times 10^{-3}$	0.008	0.024	0.032	0.024	0.026	-0.025	0.034
31.6–36.3	33.8	$(4.399 \pm 0.021^{+0.249}_{-0.186}) \times 10^{-3}$	0.011	0.000	0.032	0.024	0.026	-0.026	0.028
36.3–41.7	38.8	$(2.854 \pm 0.016^{+0.152}_{-0.119}) \times 10^{-3}$	0.010	0.000	0.032	0.024	0.024	-0.025	0.023
41.7–47.9	44.6	$(1.818 \pm 0.012^{+0.091}_{-0.075}) \times 10^{-3}$	0.010	0.000	0.032	0.024	0.023	-0.025	0.018
47.9–55.0	51.2	$(1.182 \pm 0.009^{+0.056}_{-0.049}) \times 10^{-3}$	0.011	0.000	0.032	0.023	0.021	-0.024	0.013
55.0–63.1	58.7	$(7.670 \pm 0.066^{+0.344}_{-0.318}) \times 10^{-4}$	0.011	0.000	0.032	0.021	0.018	-0.024	0.009
63.1–72.4	67.4	$(4.988 \pm 0.049^{+0.210}_{-0.206}) \times 10^{-4}$	0.010	0.000	0.032	0.019	0.016	-0.024	0.006
72.4–83.2	77.5	$(3.191 \pm 0.036^{+0.128}_{-0.135}) \times 10^{-4}$	0.012	0.000	0.032	0.017	0.013	-0.025	0.004
83.2–95.5	88.8	$(2.072 \pm 0.027^{+0.080}_{-0.089}) \times 10^{-4}$	0.012	0.000	0.032	0.015	0.010	-0.026	0.002
95.5–109.7	102.0	$(1.36 \pm 0.02^{+0.05}_{-0.06}) \times 10^{-4}$	0.013	0.000	0.032	0.012	0.007	-0.028	0.002
109.7–125.9	117.2	$(8.81 \pm 0.15^{+0.32}_{-0.40}) \times 10^{-5}$	0.013	0.000	0.032	0.010	0.004	-0.030	0.002
125.9–144.5	134.5	$(5.73 \pm 0.12^{+0.20}_{-0.27}) \times 10^{-5}$	0.014	0.000	0.032	0.008	0.002	-0.032	0.003
144.5–166.0	154.3	$(3.80 \pm 0.09^{+0.14}_{-0.19}) \times 10^{-5}$	0.014	0.000	0.032	0.005	-0.000	-0.034	0.004
166.0–190.6	177.6	$(2.54 \pm 0.07^{+0.09}_{-0.13}) \times 10^{-5}$	0.014	0.000	0.032	0.003	-0.001	-0.035	0.004
190.6–218.8	203.7	$(1.63 \pm 0.05^{+0.06}_{-0.08}) \times 10^{-5}$	0.014	0.000	0.032	0.002	-0.001	-0.035	0.004
218.8–251.2	233.7	$(1.03 \pm 0.04^{+0.04}_{-0.05}) \times 10^{-5}$	0.014	0.000	0.032	0.000	0.001	-0.034	0.003
251.2–288.4	268.5	$(6.88 \pm 0.28^{+0.25}_{-0.33}) \times 10^{-6}$	0.017	0.000	0.032	-0.001	0.003	-0.031	0.002
288.4–331.1	308.2	$(4.51 \pm 0.21^{+0.17}_{-0.20}) \times 10^{-6}$	0.018	0.000	0.032	-0.001	0.007	-0.026	-0.001
331.1–380.2	353.3	$(2.85 \pm 0.16^{+0.11}_{-0.12}) \times 10^{-6}$	0.018	0.000	0.032	-0.000	0.011	-0.020	-0.005
380.2–436.5	407.5	$(1.72 \pm 0.11^{+0.07}_{-0.07}) \times 10^{-6}$	0.019	0.000	0.032	0.001	0.017	-0.011	-0.010
436.5–501.2	466.5	$(1.12 \pm 0.07^{+0.05}_{-0.05}) \times 10^{-6}$	0.019	0.000	0.032	0.002	0.022	-0.001	-0.016
501.2–575.4	536.5	$(6.50 \pm 0.50^{+0.28}_{-0.42}) \times 10^{-7}$	$^{+0.000}_{-0.051}$	0.000	0.032	0.005	0.026	0.011	-0.022
575.4–660.7	615.3	$(4.49 \pm 0.38^{+0.24}_{-0.30}) \times 10^{-7}$	$^{+0.019}_{-0.053}$	0.000	0.032	0.009	0.030	0.023	-0.027
660.7–758.6	708.9	$(2.58 \pm 0.28^{+0.16}_{-0.18}) \times 10^{-7}$	$^{+0.019}_{-0.053}$	0.000	0.032	0.014	0.031	0.036	-0.032
758.6–871.0	809.7	$(1.87 \pm 0.22^{+0.13}_{-0.18}) \times 10^{-7}$	$^{+0.000}_{-0.083}$	0.000	0.032	0.019	0.030	0.047	-0.033
871.0–1000.0	929.9	$(1.38 \pm 0.18^{+0.10}_{-0.13}) \times 10^{-7}$	$^{+0.000}_{-0.083}$	0.000	0.032	0.026	0.026	0.056	-0.031
1000.0–1148.2	1080.5	$(9.31 \pm 1.35^{+0.81}_{-0.60}) \times 10^{-8}$	$^{+0.032}_{-0.051}$	0.000	0.032	0.036	0.017	0.063	-0.024
1148.2–1318.3	1224.8	$(4.48 \pm 0.89^{+0.41}_{-0.27}) \times 10^{-8}$	$^{+0.032}_{-0.051}$	0.000	0.032	0.044	0.006	0.065	-0.013
1318.3–1513.6	1400.8	$(1.67 \pm 0.52^{+0.19}_{-0.12}) \times 10^{-8}$	$^{+0.066}_{-0.061}$	0.000	0.032	0.055	-0.009	0.064	0.004
1513.6–1737.8	1618.3	$(1.88 \pm 0.52^{+0.22}_{-0.14}) \times 10^{-8}$	$^{+0.066}_{-0.061}$	0.000	0.032	0.069	-0.030	0.057	0.028
1737.8–1995.3	1891.3	$(1.25 \pm 0.39^{+0.17}_{-0.11}) \times 10^{-8}$	$^{+0.066}_{-0.061}$	0.000	0.032	0.085	-0.053	0.045	0.059
1995.3–2290.9	2162.0	$(3.79^{+3.08}_{-2.04}\ ^{+0.55}_{-0.76}) \times 10^{-9}$	$^{+0.032}_{-0.183}$	0.000	0.032	0.100	-0.073	0.032	0.087
2290.9–2630.3	2481.2	$(3.06^{+2.29}_{-1.37}\ ^{+0.52}_{-0.63}) \times 10^{-9}$	$^{+0.032}_{-0.183}$	0.000	0.032	0.118	-0.089	0.022	0.111
2630.3–3019.9	2873.3	$(3.13^{+2.04}_{-1.63}\ ^{+0.60}_{-0.65}) \times 10^{-9}$	$^{+0.032}_{-0.183}$	0.000	0.032	0.140	-0.096	0.020	0.124
3019.9–3467.4	3133.1	$(1.05^{+1.43}_{-0.71}\ ^{+0.22}_{-0.32}) \times 10^{-9}$	$^{+0.064}_{-0.293}$	0.000	0.032	0.153	-0.091	0.027	0.119
3467.4–3981.1	3738.3	$(9.60^{+12.67}_{-6.45}\ ^{+2.12}_{-2.88}) \times 10^{-10}$	$^{+0.064}_{-0.293}$	0.000	0.032	0.183	-0.053	0.079	0.063
3981.1–4570.9	4170.3	$(8.29^{+11.21}_{-5.60}\ ^{+2.17}_{-2.45}) \times 10^{-10}$	$^{+0.064}_{-0.293}$	0.000	0.032	0.203	-0.002	0.149	-0.020

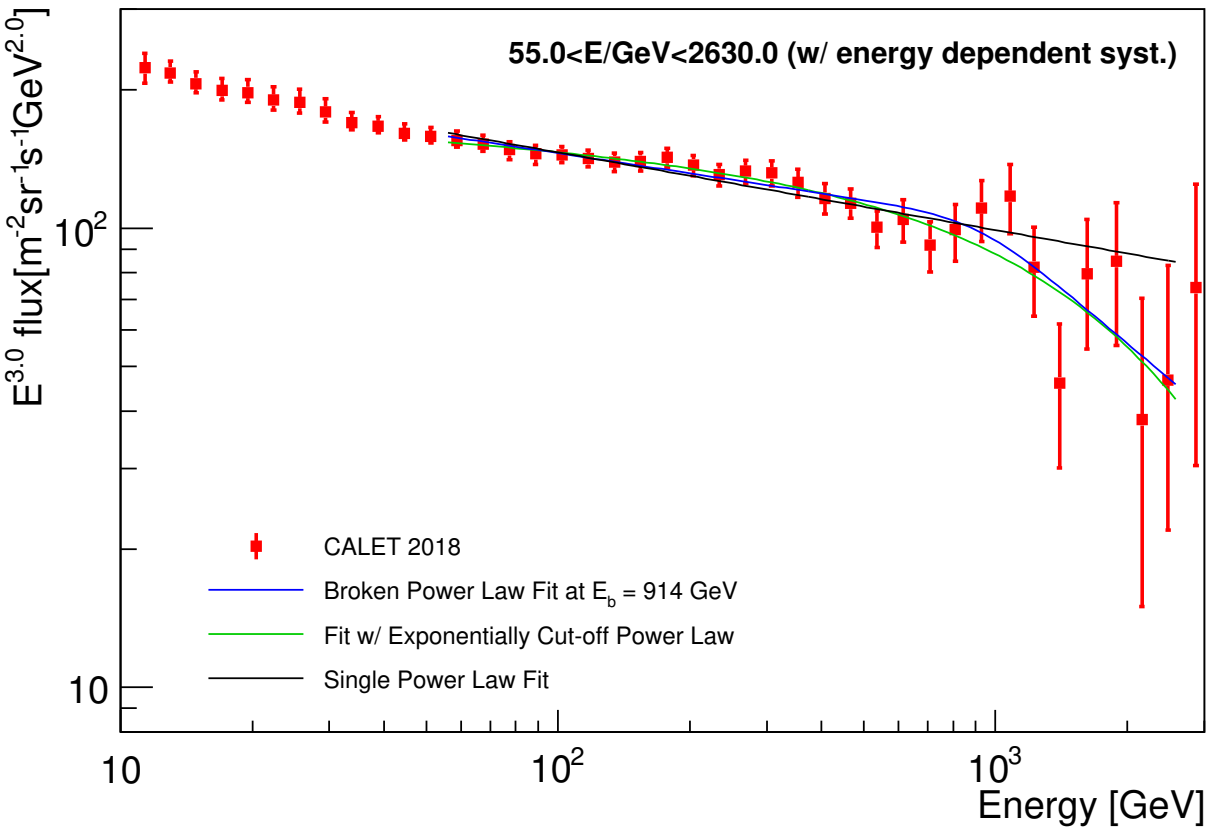

FIG. 5. The fit of the CALET all-electron spectrum with a smoothly broken power law model [1] (blue line), while fixing the break energy at 914 GeV as determined by DAMPE [1]. The smoothly broken power law model is defined as: $\Phi(E) = \Phi_0(E/100\ \mathrm{GeV})^{-\gamma_1}[1+(E/E_b)^{-(\gamma_1-\gamma_2)/\Delta}]^{-\Delta}$, where E_b is the break energy, while γ_1 and γ_2 are the power law indices below and above the break energy, respectively. The smoothness parameter, Δ, is fixed to 0.1. The fitting yields $\gamma_1 = -3.15 \pm 0.02$ and $\gamma_2 = -3.81 \pm 0.32$ with a χ^2 of 17.0 and number of degree of freedom (NDF) being 25. If we fit the spectrum with an exponentially cut-off power law [2] (green line), we obtain 2.3±0.7 TeV as the cutoff energy and a spectral index of -3.06 ± 0.03 with $\chi^2/NDF = 13.0/25$. On the other hand, a single power law fit (black line) in the same energy range gives an index of -3.17 ± 0.02 with $\chi^2/\mathrm{NDF} = 26.5/26$. All the parameters are consistent within errors between this energy binning (as shown in Table II) and our original energy binning (as shown in Table I).

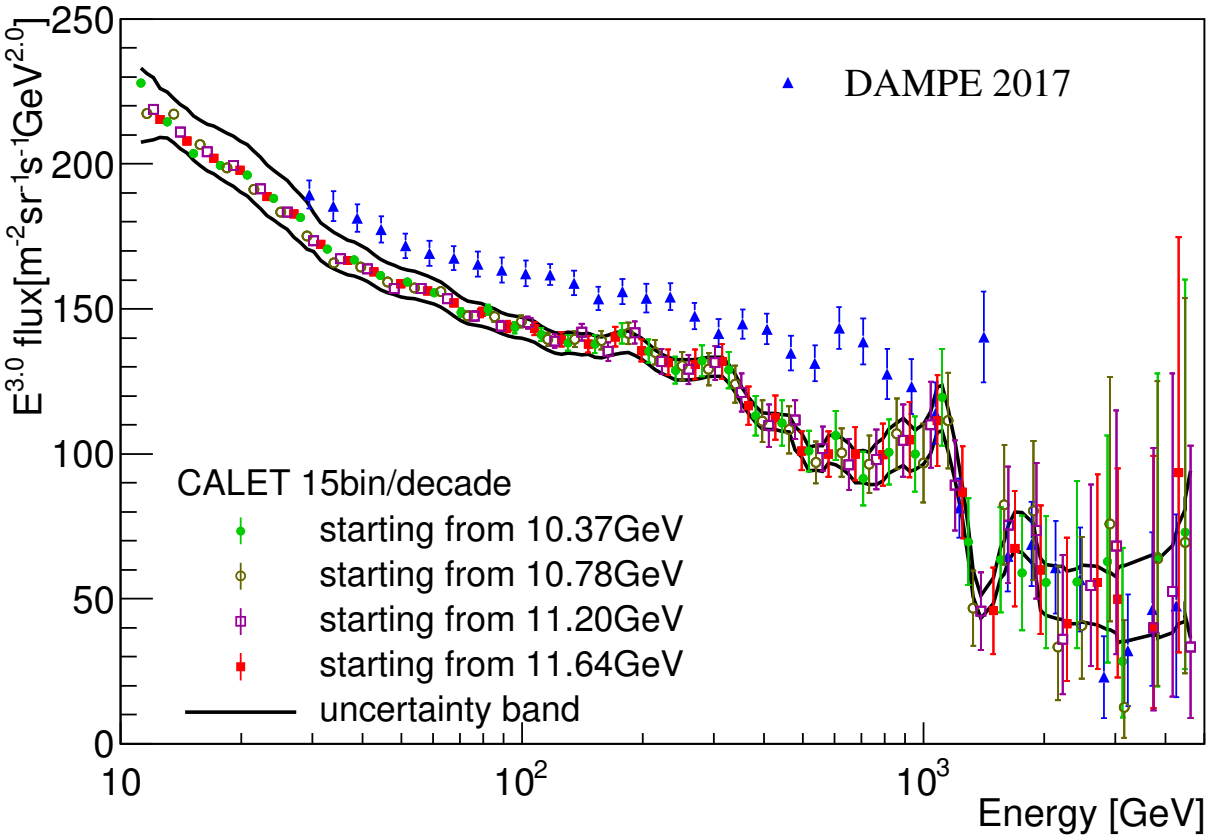

FIG. 6. Study of possible binning related effects in the CALET electron and positron spectrum. To further test the presence of potential systematics in our spectrum, different choices for the adopted binning are checked where the bin-width is chosen as 15 bins/decade in equal log-bins and four different binnings are shown in the same plot. Each binning is shifted by one fourth of the bin width to study possible binning related issues. The solid curves in the figure show the energy dependent systematic uncertainty band. Transition from event selection A+B with K-cut to A+B+C+D acceptance with BDT occurs in both cases at the low-edge of the bin containing 500 GeV. As demonstrated, the deviation due to binning is well below our energy dependent systematic uncertainty or statistical fluctuations. Therefore, bin-to-bin migration and related effects are negligible compared to our estimated systematic uncertainties, in accordance with the estimated CALET energy resolution of 2% above 20 GeV.

[1] G. Ambrosi *et al.*, Nature **552**, 63 (2017).
[2] S. Abdollahi *et al.*, Phys. Rev. D **95**, 082007 (2017).